JMEPEG
https://doi.org/10.1007/s11665-024-09909-2

1059-9495/$19.00

ORIGINAL RESEARCH ARTICLE

Preparation and Tribological Behavior of γ-AlOOH/Hexagonal Boron Nitride Composites as Additives in Water-Based Lubricant

Rui Liu, Lili He, Shangyu Li, Chunhua Ge, Wenxin Li, and Xiangdong Zhang

Submitted: 25 September 2023 / Revised: 8 April 2024 / Accepted: 15 May 2024

Recently, water-based lubricant has received extensive attention with the enhancement of environmental awareness and economic considerations. A series of novel γ-AlOOH/h-BN composites were successfully prepared by simple hydrothermal method and employed as additive to improve tribological behaviors of water-based lubricant. The morphologies of γ-AlOOH nanoparticles were influenced in different alkaline environments, which could be attributed to the formation of Al-triethylamine (Al-TEA). Furthermore, when the quantity of BN is same, the granular γ-AlOOH nanoparticles under TEA condition owing to a smaller size presented the better anti-friction property. The dispersibility and stability of BN in water were improved via loading AlOOH nanoparticles onto BN. Compared with pure BN, the nanocomposites can be stable in water for 24 h. The tribological behaviors were studied by four-ball tribological machine, the results showed that obtained samples exhibited outstanding anti-friction and anti-wear properties both in pure water and in water-glycol (mass ratio is 55%:45%) lubricant.

Keywords γ-AlOOH/h-BN, anti-friction, anti-wear, composites, water-based lubricant

1. Introduction

Friction and wear have caused various problems such as unnecessary energy wastage, environmental pollution, equipment damage and so on (Ref 1-4). Therefore, controlling friction and wear are treated as a crucial strategy for protecting the environment and improving energy efficiency (Ref 5, 6). Recently, many materials like lubricants were designed and used to reduce the friction and wear (Ref 7-11). Thereinto, synthetic oil and mineral oils are difficult to degrade in nature as oil lubricant (Ref 12). Compared with the oil lubricants, water-based lubricants have many unique advantages like high compatibility with the environment, low cost and good environmental compatibility (Ref 13, 14). However, water-based lubricant has poor tribological properties, which can be effectively improved by introducing functional additives to water-based lubricant. Lubricant additives improve the bearing capacity and oxidation resistance, reduce friction and reduce wear (Ref 15). Xiong et al. (Ref 16) synthesized N-containing heterocyclic imidazoline compounds which improved tribological performances of the water-glycol.

Two-dimensional (2D)-layered materials incorporating graphene, transition metal dichalcogenides (TMDs), MXene (Ti_3C_2) and hexagonal boron nitride (h-BN) have drawn enormous attention because of the excellent tribological behaviors (Ref 17-19). Additionally, BN has become a promising candidate in tribological filed owing to its splendid thermal conductivity performance, chemical stability, electrical insulation property and low friction coefficient. BN mainly consisted of B and N atoms which are connected via strong covalent bond. The layers of h-BN are connected by weak Van der Waals forces, making it easier to shear along base surface of wafer layer structure under sliding pressure (Ref 20, 21). During the process of slide, h-BN can enter the contact rubbing areas and then avoid the direct contact of friction pairs, friction and wear are effectively reduced (Ref 22-24). However, BN is poorly dispersed in water-based lubricants, which remains a challenge (Ref 25).

Many inorganic nanoparticles possess small particle size so that they can fill with micro-roughness (Ref 26). In the meantime, nanoparticles may precipitate and form protective film ascribed to the high surface energy, they also owe the effect of repairing or self-repairing on the worn surfaces (Ref 27). Metal oxide nanoparticles have been proved to have good anti-friction effect. Wang et al. (Ref 28) successfully synthesized Fe_3O_4 with different morphologies (nanospheres, nanowires and nanosheets), which can effectively improve its tribological properties when used as an additive to liquid paraffin. Zhao et al. (Ref 29) used the hydrothermal method to prepare water-soluble CuO nanoparticles with different morphologies (nanobelt, nanorod and spindle). As a water-based lubricant additive, CuO nanoparticles can enter the friction surface to form a friction protective film, which can prevent the direct contact of the friction pair. In addition, dispersing the nanoparticles onto the 2D-layered material can improve the agglomeration of the nanoparticles. At the same time, the dispersibility of 2D-layered materials was improved in the lubricant (Ref 30).

Rui Liu, Lili He, Shangyu Li, Chunhua Ge, Wenxin Li, and **Xiangdong Zhang**, College of Chemistry, Liaoning University, Chongshan Road No. 66, Shenyang 110036, People's Republic of China. Contact e-mail: xd623@sina.com.

Published online: 12 August 2024

Herein, we successfully prepared a series of novel γ-AlOOH/h-BN composites employed the simple hydrothermal methods to load the γ-AlOOH nanoparticles onto the h-BN. The structures and surface morphologies of γ-AlOOH/h-BN samples were verified by FTIR, XRD, SEM and TEM. Then, the tribological properties of γ-AlOOH/h-BN samples were studied as additives in water and water-glycol, respectively. In consequence, this paper provided a feasible strategy for preparing water-based lubricant additives.

2. Experimental Sections

2.1 Materials and Reagents

Hexagonal boron nitride (h-BN) was bought from Tianyuan Chemical Research Institute. Potassium hydroxide (KOH), aluminum nitrate hydrate ($Al(NO_3)_3{\cdot}9H_2O$), triethylamine (TEA) and sodium citrate were gained from Sinopharm Chemical Reagent Co. Ltd. Cetyltrimethyl ammonium bromide (CTAB) was obtained from Beijing Aoboxing Biotechnology Co. Ltd. All chemicals were analytic grade and for direct use.

2.2 Preparation of γ-AlOOH/h-BN

The sodium citrate and CTAB (molar ratio 1:2) were dissolved into 70 mL deionized water and then stirred for 20 min. Then, 3.5 g of $Al(NO_3)_3{\cdot}9H_2O$ was added to the solution and stirred until it completely dissolved. The 0.18 g, 0.26 g, 0.35 g, 0.48 g and 0.7 g of h-BN powders were dispersed to the above solution and ultrasonicated for 3 h; then, dispersed solution A was obtained. Finally, the KOH and TEA were used to provide alkaline environment, respectively.

The 2.35 g of KOH was dissolved in 5 mL deionized water and added to the dispersed solution A. After stirring at 50 °C for 45 min, the mixtures were transferred to the 100 mL PTFE reactors and heated at 180 °C for 15 h. After the reaction finished, the products were washed with deionized water and ethanol. The γ-AlOOH/h-BN (**1-5**) samples were obtained after drying at 60 °C for 12 h in the oven. The pure γ-AlOOH (**1**) nanoparticles were prepared under the same condition without BN. The reactions in hydrothermal process are as follows:

$$Al^{3+} + 3OH^- \rightarrow Al(OH)_3 \quad \text{(Eq 1)}$$

$$Al(OH)_3 \rightarrow AlOOH + H_2O \quad \text{(Eq 2)}$$

The appropriate amount of TEA was slowly added to the dispersed solution A until the pH reached 11. After stirring at room temperature for 30 min, the mixture was transferred to the 100 mL PTFE reactors and heated at 190 °C for 20 h. After the reaction finished, the products were washed with deionized water and ethanol. The γ-AlOOH/h-BN (**6-10**) samples were obtained after drying at 60 °C for 12 h in an oven. The pure AlOOH (**2**) nanoparticles were gained using the method. The reactions in hydrothermal process are as follows:

$$Al^{3+} + TEA \rightarrow [Al - TEA]^{3+} \quad \text{(Eq 3)}$$

$$[Al - TEA]^{3+} + 3OH^- \rightarrow Al(OH)_3 + TEA \quad \text{(Eq 4)}$$

$$Al(OH)_3 \rightarrow AlOOH + H_2O \quad \text{(Eq 5)}$$

2.3 Characterization

The chemical bonds of pure h-BN, γ-AlOOH and γ-AlOOH/h-BN composites were investigated by Fourier transform infrared spectra (FTIR, TENSOR-27, Perkin Elmer, USA); the KBr was used as the matrix (4000-400 cm^{-1}). Phase and crystallization of prepared composite materials were surveyed by X-ray diffraction analysis (XRD, AXIS D8, Bruke, Germany). Scanning electron microscopy (SEM, SU8000, JEOL, Japan) was employed to investigate the surface morphology of composites. Transmission electron microscopy (TEM, JEM-2100, JEOL, Japan) was used to further confirm the size and morphologies of the composites.

2.4 Tribological Test

The tribological behaviors of water and water-glycol (mass ratio 55%:45%) with γ-AlOOH/h-BN (**1-10**) were characterized via tribological test. Water-based lubricants with γ-AlOOH/h-BN (**1-10**) additives were prepared at concentration 0.03, 0.06, 0.09, 0.12 and 0.15 wt.%. The average COF was obtained by using a four-ball friction tester (MMW-1A, Jinan Yihua, China). The friction pair was consisted by an upper ball, three lower balls (Φ = 12.7 mm, GCr15). Before the test started, the steel balls were cleaned by acetone ultrasonic for 30 min to remove surface contamination. Then, 8 mL of lubricant was added until the friction surfaces could be covered. The tribological performance tests were proceed at room temperature with 100 N load and test duration of 30 min; rotation speed was set to 120 r/min. The morphologies and WSD of three bottom balls were observed by YW MS2300D optical microscope with ± 0.01 mm accuracy. All tribological tests were repeated three times to obtain mean value under the same test conditions.

3. Results and Discussion

3.1 FTIR Analysis

The FTIR spectra of h-BN and γ-AlOOH nanoparticles and γ-AlOOH/h-BN (**1-10**) are shown in Fig. 1. The characteristic peaks at 3300 and 3086 cm^{-1} belong to symmetric and asymmetric stretching vibrations of Al-OH. The shoulder peak of 1165 cm^{-1} is related to symmetric and asymmetric bending vibrations of Al-OH. The tensile vibration absorption peak of Al-O-Al was located at 1070 cm^{-1}. The peaks at 742, 619 and 492 cm^{-1} were associated to the vibration of AlO_6 octahedron modes, which corresponded to torsional vibrations, stretching vibration and bending stretching vibration of Al-O, respectively (Ref 31-33). The 1632 cm^{-1} belongs to bending vibrations of O-H (surface adsorbed H_2O molecule) (Ref 34). The peak of 1369 and 816 cm^{-1} was ascribed to the in-plane stretching vibration absorption peak of BN and out-of-plane bending vibration absorption peak of BN (Ref 35, 36), respectively. As the BN addition increased, the characteristic peaks intensity of BN gradually increased, while peak intensity of γ-AlOOH

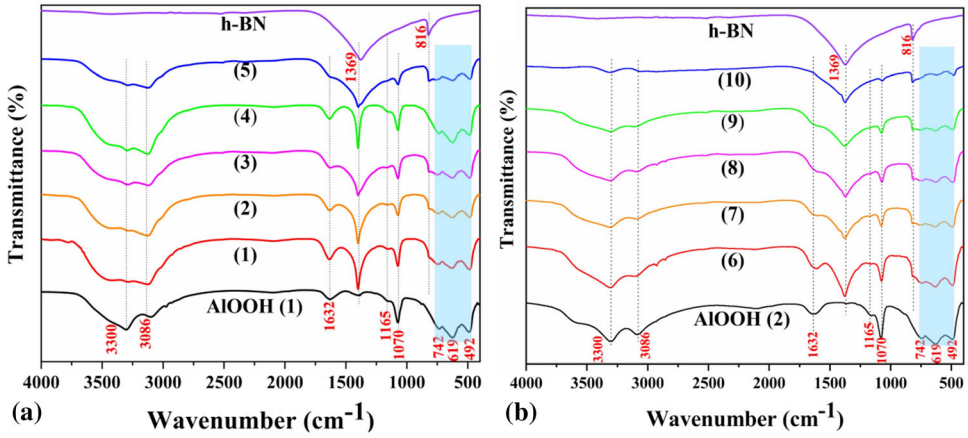

Fig. 1 FTIR spectra of (a) h-BN, γ-AlOOH (**1**), γ-AlOOH/h-BN (**1-5**) and (b) h-BN, γ-AlOOH (**2**), γ-AlOOH/h-BN (**6-10**)

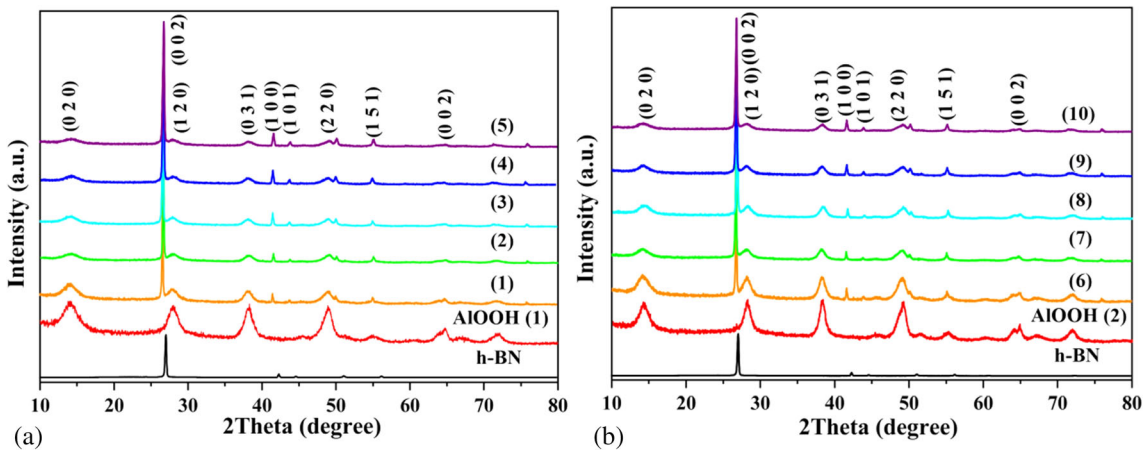

Fig. 2 XRD patterns of (a) h-BN, γ-AlOOH (**1**), γ-AlOOH/h-BN (**1-5**) and (b) h-BN, γ-AlOOH (**2**), γ-AlOOH/h-BN (**6-10**)

gradually decreased, which indicated that the loading of γ-AlOOH particles on the surface of h-BN would be influenced by quantity of BN.

3.2 XRD Analysis

Figure 2 exhibited XRD patterns of h-BN, γ-AlOOH, γ-AlOOH/h-BN (**1-10**) samples. As the figure shown, the peaks at 2θ = 14.28°, 28.15°, 38.55°, 49.19°, 55.17° and 64.9° could be observed, which were corresponded to the crystal plane diffraction peaks of (020), (120), (031), (220), (151) and (002) of orthorhombic structure γ-AlOOH (JCPDS card no. 021-1307), respectively (Ref 34, 37). The characteristic diffraction peaks at 2θ = 26.79°, 41.69°, 43.84° corresponded to (002), (100), (101) three diffraction crystal planes of h-BN (JCPDS No. 34-0421), respectively (Ref 36, 38, 39). XRD results are consistent with FTIR spectra, indicating that γ-AlOOH is successfully loaded onto h-BN.

3.3 Morphology Analysis of γ-AlOOH/h-BN (1-10)

Figure 3 showed the SEM pictures of the γ-AlOOH nanoparticles and γ-AlOOH/h-BN (**1-10**) composites. The h-BN demonstrated stacked sheet structure with a diameter of about 8-10 μm, while γ-AlOOH particles under different alkaline conditions all presented nanoscale size. There are obvious differences in morphology, γ-AlOOH (**1**) nanoparticles exhibited thin nanosheet structure and were prone to agglomerate randomly in Fig. 3(a), but γ-AlOOH (**2**) nanoparticles showed granular morphology of agglomeration (Fig. 3g). The surface of γ-AlOOH/h-BN (**1-10**) samples became obviously rough than pure BN sheet, indicating that the γ-AlOOH nanoparticles were successfully loaded on the BN sheet. Indeed, the γ-AlOOH nanoparticles were more uniformly distributed and relatively more dispersed on the BN sheet in contrast to pure AlOOH. Meantime, the size and morphology of AlOOH nanoparticles did not change significantly even loading on BN. Additive amount of BN only has an effect of loading capacity of the γ-AlOOH nanoparticles on BN sheet.

For γ-AlOOH/h-BN (**1-5**) composites, distribution of γ-AlOOH was gradually altered from multi-layer packing to single layer as the amount of BN increased. The γ-AlOOH nanoparticles achieved the optimum dispersion in AlOOH/h-BN (**4**) sample (Fig. 3e). As the amount of BN further increased, the quantity of AlOOH (**1**) nanoparticles loading on BN decreases. It could be attributed that the number of nanoparticles is not sufficient to support their formation of single-layer distribution over more BN sheets. The distributed condition of γ-AlOOH nanoparticles on BN in γ-AlOOH/h-BN (**6-10**) samples could be observed (Fig. 3g-l). Similarly, γ-AlOOH nanoparticles could be loaded on BN sheet as addition

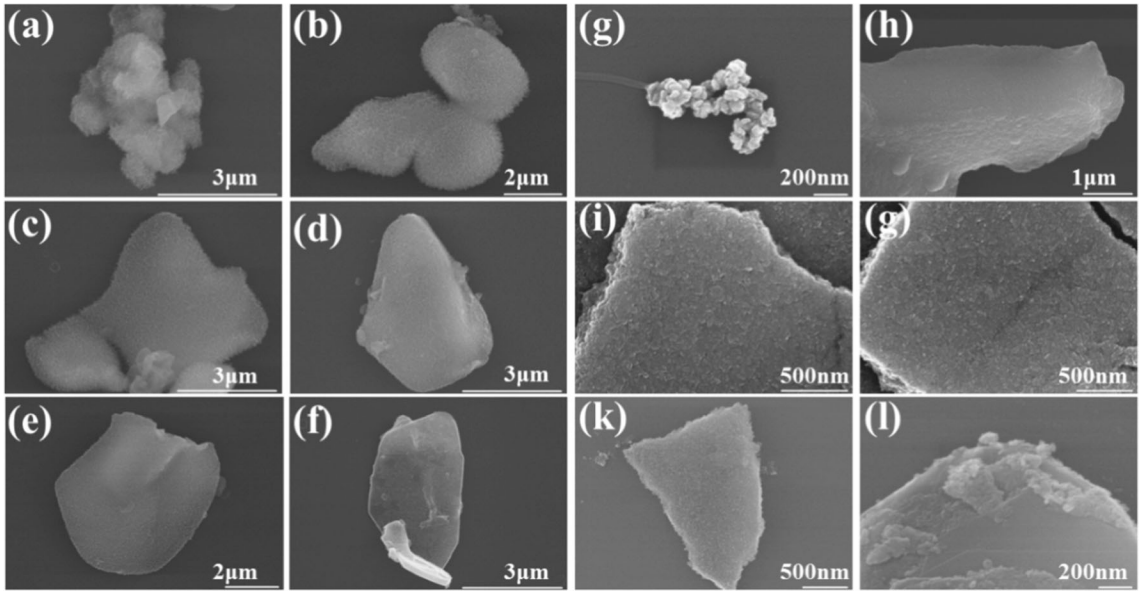

Fig. 3 SEM images of (a) γ-AlOOH (**1**), (b-f) γ-AlOOH/h-BN (**1-5**), (g) γ-AlOOH (**2**) and (h-l) γ-AlOOH/h-BN (**6-10**)

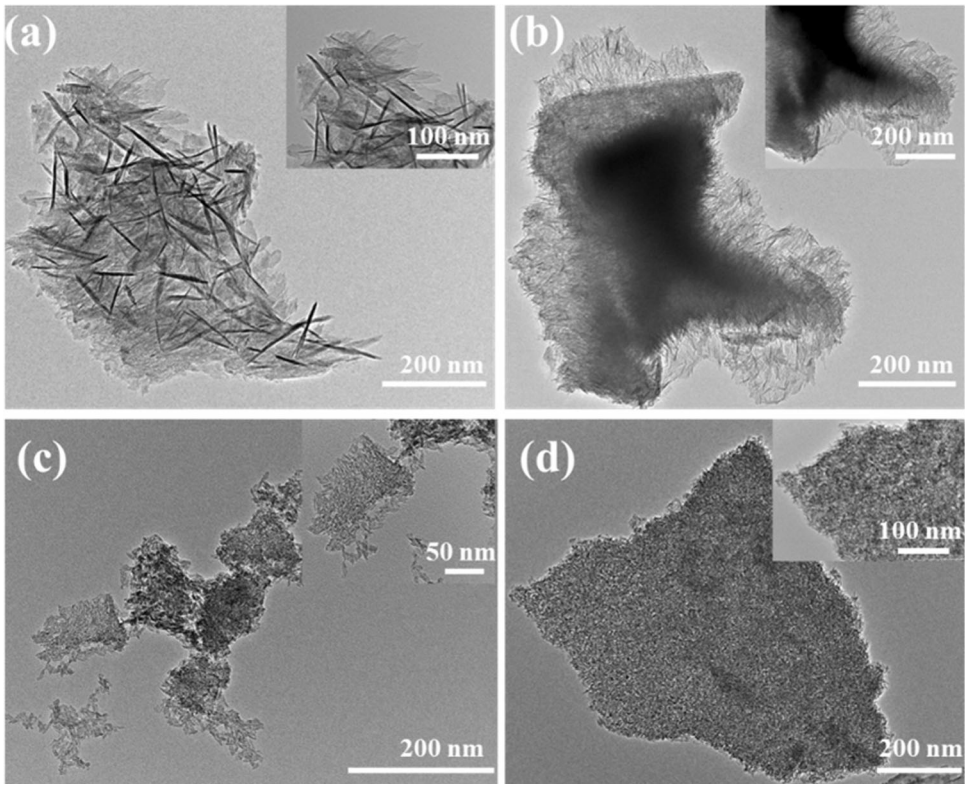

Fig. 4 TEM images of (a) γ-AlOOH (**1**), (b) γ-AlOOH/h-BN (**4**), (c) γ-AlOOH (**2**) and (d) γ-AlOOH/h-BN (**9**)

of BN and evenly dispersed on the surface of BN. The γ-AlOOH (**2**) particles were in an optimal state of dispersion at the Fig. 3(K). As the amount of h-BN continued to increase, the γ-AlOOH nanoparticles which loaded on BN sheets decrease. SEM pictures confirmed that γ-AlOOH was successfully loaded on BN sheets, and different bases had a great impact on morphology of AlOOH nanoparticles. The addition of BN did not change the size and morphology of nanoparticles, but dispersion state was affected with the amount of BN addition.

Figure 4 showed TEM images of γ-AlOOH (**1**), γ-AlOOH (**2**), γ-AlOOH/h-BN (**4**) and γ-AlOOH/h-BN (**9**) samples. As shown in Fig. 4(a), γ-AlOOH (**1**) nanoparticles were irregular folded sheet with the diameter of about 100 nm. Due to the different orientations of each sheet, the particle clusters

presented a two-dimensional sheet stacking state. After loaded on BN (Fig. 4b), γ-AlOOH (**1**) nanoparticles were orderly distributed to BN surface with the single layer, which is in accordance with Fig. 3(e). The morphology of γ-AlOOH (**2**) nanoparticles presented long granular structure with the single particle length of about 20 nm, which shown in Fig. 4(c). Similarly, it can be clearly found in Fig. 4(d) that the particles were evenly distributed on the BN sheet.

3.4 Dispersion and Stability Analysis

Figure 5 showed the dispersion of composites at the concentration of 0.06 wt.% in water-based lubricant. It could be observed that the composites were relatively evenly dispersed in the water-based lubricant at first. After 12 h, all the other γ-AlOOH/h-BN (**1-5**) samples agglomerated and settled completely except γ-AlOOH/h-BN (**3**) in the water. The γ-AlOOH/h-BN (**6-10**) agglomerated and settled completely in the water after 24 h, because of the γ-AlOOH (**2**) have smaller size in comparison with γ-AlOOH (**1**). The γ-AlOOH/h-BN (**1-10**) agglomerated and settled completely in the water-glycol after 24 h. The prepared samples all presented the excellent dispersibility.

3.5 Tribological properties in different lubricants

Figure 6(a-b) displayed the average COFs of γ-AlOOH/h-BN (**1-10**) composites additives with the concentration of 0.03-0.15 wt.% at 100 N loading. The average COFs of the γ-AlOOH/h-BN (**1-10**) were all lower than that of pure water, which indicated γ-AlOOH/h-BN (**1-10**) samples have significant friction-reducing property in water as lubricant additives (shown in Fig. 6). At the same time, it is not difficult to find that the average COFs of the γ-AlOOH/h-BN (**1-10**) samples decreased first and then increased as the concentration increased. According to Fig. 6(a), when the additive concentration of γ-AlOOH/h-BN (**2**) sample in water was 0.12%, the average COF value reached minimum which was 0.250. The average COF was reduced by 37.58% than pure water, which showed the best anti-friction effect in γ-AlOOH/h-BN (**1-5**)

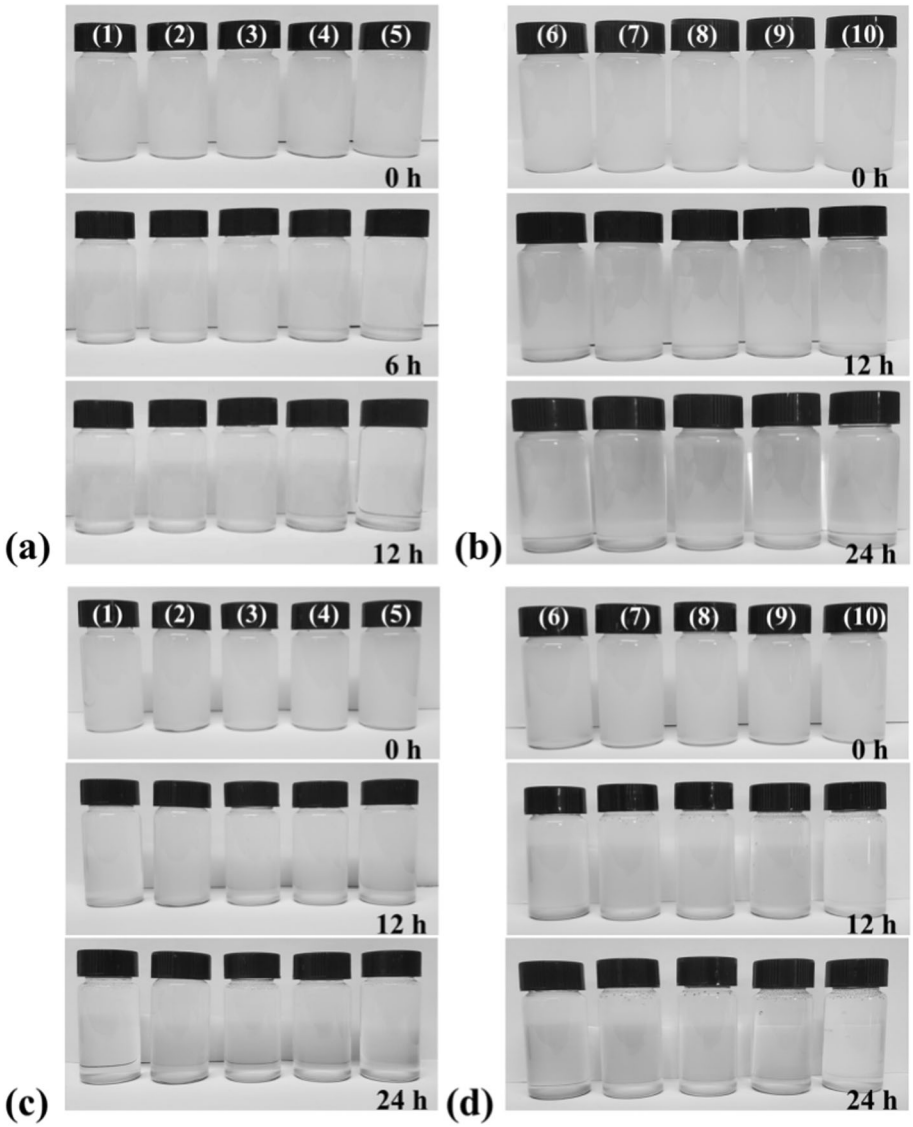

Fig. 5 The optical pictures of (a-b) γ-AlOOH/h-BN (**1-10**) in water and (c-d) γ-AlOOH/h-BN (**1-10**) in water-glycol at the concentration of 0.06 wt.%

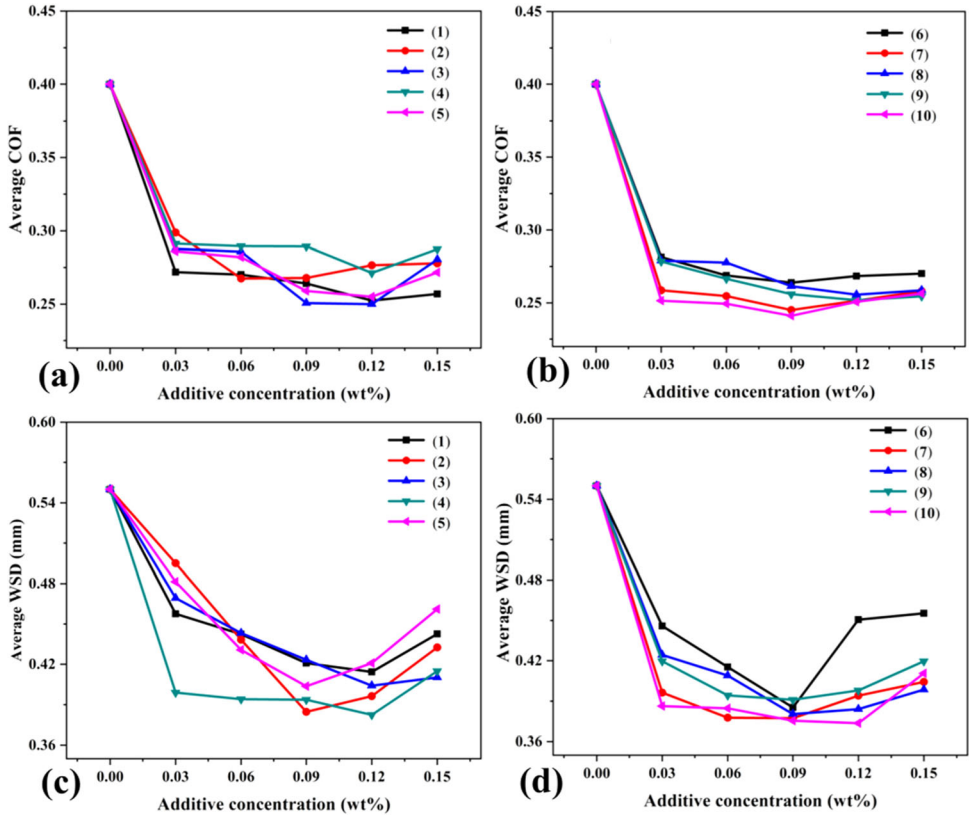

Fig. 6 Average COFs of (a) γ-AlOOH/h-BN (**1-5**), (b) γ-AlOOH/h-BN (**6-10**), average WSDs of (c) γ-AlOOH/h-BN (**1-5**) and (d) γ-AlOOH/h-BN (**6-10**) in water

samples. In γ-AlOOH/h-BN (**6-10**) samples, γ-AlOOH/h-BN (**10**) exhibited the best anti-friction effect. γ-AlOOH/h-BN (**10**) had the minimum average COF value of 0.241 at the additive concentration 0.09 wt.% (shown in Fig. 6b), which is 41.20% lower than that without additive in this serious of composites.

The average WSDs of γ-AlOOH/h-BN (**1-10**) additives are showed in Fig. 6(c-d), which showed a similar trend to the average COF. The average WSDs of γ-AlOOH/h-BN (**1-10**) were also less than that of pure water, indicating γ-AlOOH/h-BN (**1-10**) samples have outstanding anti-wear property as lubricant additives. The average WSDs of γ-AlOOH/h-BN (**4**) at concentration 0.12 wt.% reached the minimum value of 0.382 mm, which was reduced by 30.54% compared with the average WSD in pure water. According to the Fig. 6(d), the average WSDs of γ-AlOOH/h-BN (**10**) reached the minimum value of 0.374 mm, which was 32.06% lower than the average WSD in pure water, which showed excellent anti-wear effect.

Figure 7 displayed the average COFs of γ-AlOOH/h-BN (**1-10**) composites containing the concentration of 0.03-0.15 wt.% in the water-glycol (mass ratio 55%:45%) at 100 N loading. It could be known that the average COFs of the γ-AlOOH/h-BN (**1-10**) were completely less than that of lubricant, which suggested γ-AlOOH/h-BN (**1-10**) additives show outstanding anti-friction behavior in lubricant. In the meantime, it worth noting that the average COFs of the γ-AlOOH/h-BN (**1-10**) samples presented the trend of first decreasing and then increasing. When additive concentration of γ-AlOOH/h-BN (**1**) sample in water-glycol was 0.09 wt.%, the average COF value reached minimum which was 0.0936 (Fig. 7a). Compared with the water-glycol, the average COF was reduced by 55.44%, which showed the best anti-friction effect in γ-AlOOH/h-BN (**1-5**) samples. As could be seen in Fig. 7(b), γ-AlOOH/h-BN (**10**) had the minimum COF value of 0.0972 at the additive concentration 0.12 wt.% in the γ-AlOOH/h-BN (**6-10**) samples. Compared with lubricant, the COF was reduced by 53.72%, exhibiting the best anti-friction effect in γ-AlOOH/h-BN (**6-10**) samples.

The average WSDs of γ-AlOOH/h-BN (**1-10**) additives in water-glycol are demonstrated in Fig. 7(c-d) with different concentrations at 100 N loading. Fig. 7(c) showed that the average WSDs of γ-AlOOH/h-BN (**1-10**) were all smaller than that of water-glycol, exhibiting the outstanding anti-wear behavior of γ-AlOOH/h-BN (**1-10**) samples as lubricant additives. The average WSDs of γ-AlOOH/h-BN (**5**) at concentration 0.12 wt.% reached the minimum value of 0.333 mm, which was reduced by 39.45% compared with the average WSDs in pure water-glycol. According to Fig. 7(d), the average WSDs of γ-AlOOH/h-BN (**6**) reached the minimum value of 0.344 mm, displaying splendid anti-wear performance. Average WSDs was 37.45% lower than the average WSD of water-glycol.

The wear surface morphologies of γ-AlOOH/h-BN (**4**) and γ-AlOOH/h-BN (**10**) are exhibited in Fig. 8 at 0.03-0.15 wt.% concentration. The friction surface has many grooves and scratches after pure water lubrication, which was caused by the poor strength of the protective film formed by water on the friction surface (Fig. 8a). When γ-AlOOH/h-BN (**4**) and γ-AlOOH/h-BN (**10**) were used as additive of water, the wear scar of the friction surface was significantly relieved in various degrees. The wear scar obviously became shallower, and the

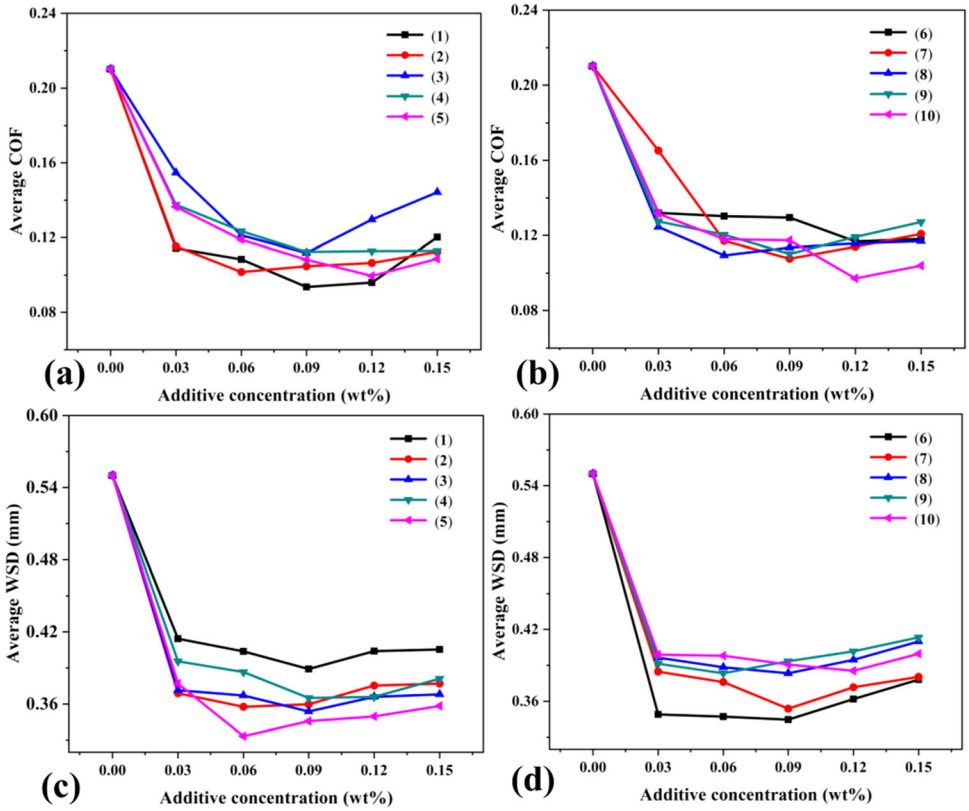

Fig. 7 Average COFs of (a) γ-AlOOH/h-BN (**1-5**), (b) γ-AlOOH/h-BN (**6-10**), average WSDs of (c) γ-AlOOH/h-BN (**1-5**) and (d) γ-AlOOH/h-BN (**6-10**) in water-glycol

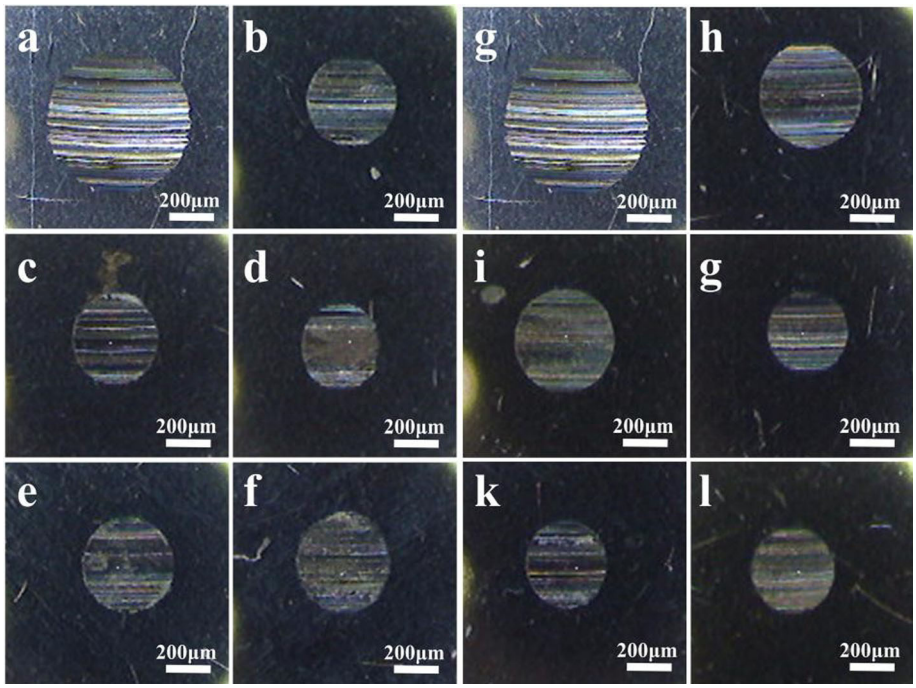

Fig. 8 Wear surface micrograph of (a, g) water, (b-f) γ-AlOOH/h-BN (**4**) and (h-l) γ-AlOOH/h-BN (**10**) in water

worn surface became smoother. Meanwhile, the WSD was all obviously reduced, which was consistent with the trend shown in Fig. 6(c-d).

Figure 9 demonstrated the worn surface morphologies of γ-AlOOH/h-BN (**5**) and γ-AlOOH/h-BN (**6**) at 0.03-0.15 wt.% water-glycol concentration. According to Fig. 9(a), the grooves and scratches improved compared with pure water, which was attributed to addition of glycol. After γ-AlOOH/h-BN (**5**) and γ-AlOOH/h-BN (**6**) were added to the lubricant, the wear scar of the friction surface was shallower and the surface became

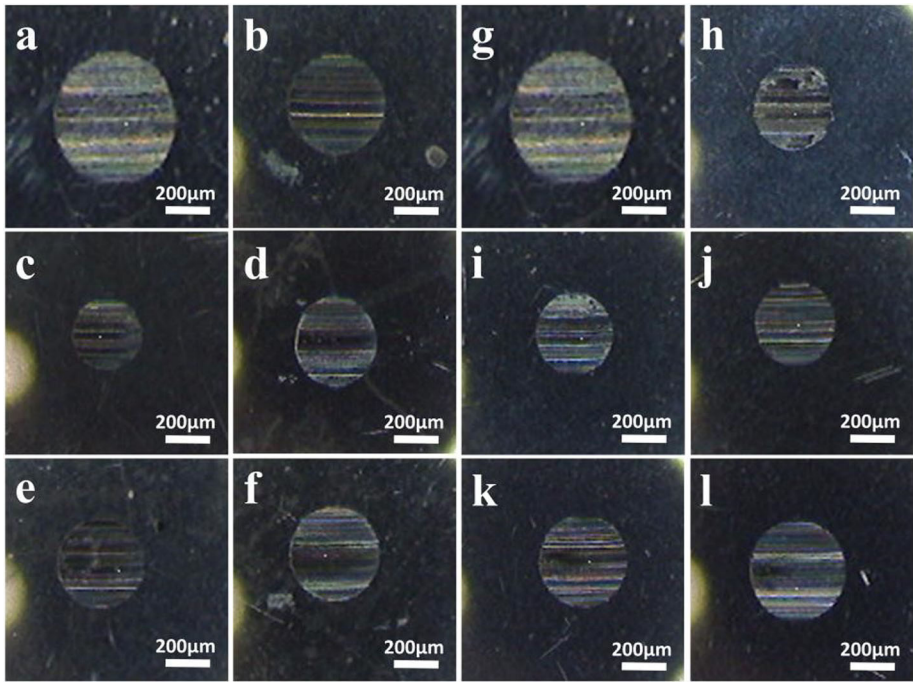

Fig. 9 Wear surface micrograph of (a, g) water-glycol, (b-f) γ-AlOOH/h-BN (**5**) and (h-l) γ-AlOOH/ h-BN (**6**) in water-glycol

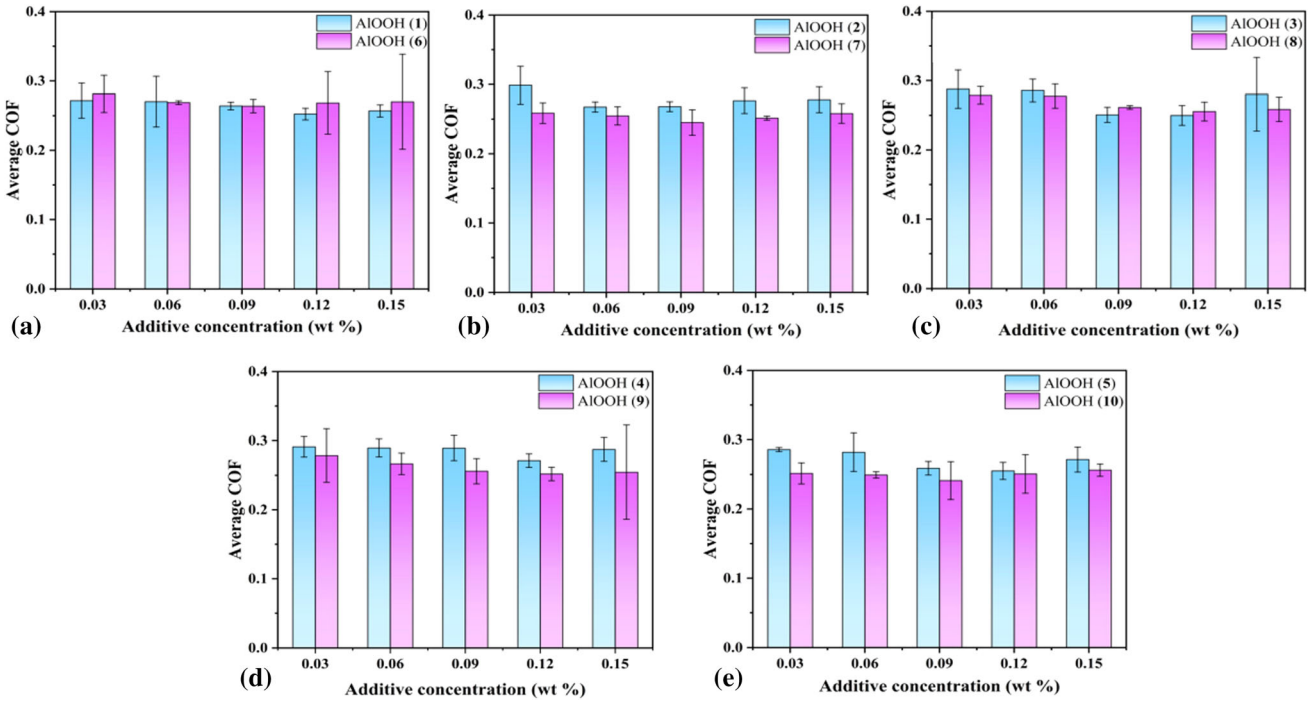

Fig. 10 Average COF of γ-AlOOH/h-BN under the same amount of h-BN

smoother. Meanwhile, the variation trend of the WSD is consistent with Fig. 7(c-d).

Figure 10 displayed comparison of average COF values of γ-AlOOH/h-BN composites at the same BN addition amount. According to Fig. 10, the average COF of γ-AlOOH/h-BN prepared under TEA is basically less than γ-AlOOH/h-BN prepared under KOH when addition quantity of BN is same. This may be caused that the BN enters the frictional pairs at the beginning and then penetrates into the grooves which formed the protective films because of the intrinsic lamellar structure (Ref [40-42]). Subsequently, the direct contact of friction surfaces was avoided. The rich -OH groups provided by γ-AlOOH render the composites to better adsorb on the surface of friction, causing the protective film more complete. Furthermore, γ-AlOOH nanoparticles further improve the dispersion and stability of h-BN in water-based lubricant, which makes protective film more stable on the friction pair. The addition of nanoparticles also improved the bearing capacity of 2D

Table 1 Comparison of reduction of average COF for different composites

Materials	Lubricant	Reduction of COF, %	References
Fe_3O_4/MoS_2	Water	34.60	(Ref 30)
AlOOH/GO	Hydroisomerization base oil (VHVI8)	14.00	(Ref 43)
SiO_2/GO	Water-based	20.70	(Ref 46)
AlOOH/BN	Water-based	55.46	Present work

materials, the excellent anti-friction and anti-wear properties of composites may be ascribed synergistic effect of nanoparticles and 2D layer material on the frictional interfaces (Ref [43-45]). Therefore, when BN quantity is same, γ-AlOOH nanoparticles plays a decisive role in friction. γ-AlOOH (**2**) has smaller size and granular morphology, resulting in the easier access to the friction surface and possessing the smaller average COF.

Table 1 shows the Comparison of Reduction of average COF for different composites. Through comparison, it can be seen that composites synthesized by us showed better anti-friction effect in the water-based lubricant.

4. Conclusion

In conclusion, a series of γ-AlOOH/h-BN samples were successfully synthesized by hydrothermal method. Morphologies of the γ-AlOOH nanoparticles were adjusted by using KOH and TEA to provide different kinds of OH^-, respectively. The obtained γ-AlOOH/h-BN samples could be used as water-based lubricant additive because the γ-AlOOH possessed the abundant -OH group. Meantime, all γ-AlOOH/h-BN composites could significantly improve the anti-friction and anti-wear properties of water-based lubricant. The tribological properties depend on the synergistic lubrication between γ-AlOOH and h-BN, the uniform dispersion of γ-AlOOH on the surface of the BN is also beneficial to the formation of a stable friction protective film.

Competing interest

The authors declare that they have no known competing financial interests or personal relationships that could have appeared to influence the work reported in this paper.

References

1. Y. Su, B. Wang, and J.J. Zou, Tribological Characteristics of Nanofluid Composite Electrostatic Spraying (NCES) in Sliding Friction, *Tribol. Int.*, 2023, **183**, p 108380. https://doi.org/10.1016/j.triboint.2023.108380
2. Q.Q. Zhang, X.G. Hu, and Y.G. Meng, Understanding of the Tribological Behaviors of Magnetic Lubrication Particle Under Magnetic Field, *Tribol. Int.*, 2022, **176**, p 107931. https://doi.org/10.1016/j.triboint.2022.107931
3. Y.W. Hu, Y.X. Wang, C.T. Wang, Y.W. Ye, H.C. Zhao, J.L. Li, X.J. Lu, C.L. Mao, S.J. Chen, J.M. Mao, L.P. Wang, and Q.J. Xue, One-Pot Pyrolysis Preparation of Carbon Dots as Eco-friendly Nanoadditives of Water-Based Lubricants, *Carbon*, 2019, **152**, p 511-520. https://doi.org/10.1016/j.carbon.2019.06.047
4. Y. Chen, K. Yang, H.B. Lin, F.Z. Zhang, B.Y. Xiong, H.L. Zhang, and C.H. Zhang, Important Contributions of Multidimensional Nanoadditives on the Tribofilms: From Formation Mechanism to Tribological Behaviors, *Compos. B*, 2022, **234**, p 109732. https://doi.org/10.1016/j.compositesb.2022.109732
5. M.H. Rahman, H. Warneke, H. Webbert, J. Rodriguez, E. Austin, K. Tokunaga, D.K. Rajak, and P.L. Menezes, Water-Based Lubricants: Development, Properties, and Performances, *Lubricants*, 2021, **9**(8), p 73. https://doi.org/10.3390/lubricants9080073
6. G.Q. Liu, X.L. Wang, F. Zhou, and W.M. Liu, Tuning the Tribological Property with Thermal Sensitive Microgelsfor Aqueous Lubrication, *ACS Appl. Mater. Interfaces*, 2013, **5**(21), p 10842-10852. https://doi.org/10.1021/am403041r
7. J.J. Chen, Q.C. Sun, J. Chen, J. Cheng, S.Y. Zhu, and J. Yang, Mechanical and Tribological Properties of h-BN/ZrO_2/SiC Solid-Lubricating Ceramic Composites, *Tribol. Int.*, 2021, **160**, p 107061. https://doi.org/10.1016/j.triboint.2021.107061
8. L.P. Wu, Y. Zhong, H.Y. Yuan, H. Liang, F. Wang, and L. Gu, Ultra-dispersive Sulfonated Graphene as Water-Based Lubricant Additives for Enhancing Tribological Performance, *Tribol. Int.*, 2022, **174**, p 107759. https://doi.org/10.1016/j.triboint.2022.107759
9. J.T. Li, C. Zhai, H.B. Yin, A.L. Wang, and L.Q. Shen, Impact of Polydimethylsiloxanes on Physicochemical and Tribological Properties of Naphthenic Mineral Oil (KN 4010)-Based Titanium Complex Grease, *Chin. J. Chem. Eng.*, 2019, **27**(4), p 944-948. https://doi.org/10.1016/j.cjche.2018.09.002
10. W.J. Bartz, Ecotribology: Environmentally Acceptable Tribological Practices, *Tribol. Int.*, 2006, **39**(8), p 728-733. https://doi.org/10.1016/j.triboint.2005.07.002
11. R.Z. Wang, C.F. Sun, X.Y. Yan, T.Y. Guo, W.J. Xiang, Z.Z. Yang, Q.L. Yu, B. Yu, M.R. Cai, and F. Zhou, Influence of the Molecular Structure on the Tribological Properties of Choline-Based Ionic Liquids as Water-Based Additives Under Current-Carrying Lubrication, *J. Mol. Liq.*, 2023, **369**, p 120868. https://doi.org/10.1016/j.molliq.2022.120868
12. W.W. Tang, Y. Wang, X.Y. Zhu, Z. Zhang, W. Zhu, H.D. Liu, W. Gao, and Y.F. Li, Graphitic Carbon Nitride Quantum Dots as Novel and Efficient Friction-Reduction and Anti-wear Additives for Water-Based Lubrication, *Wear*, 2023, **528-529**, p 204950. https://doi.org/10.1016/j.wear.2023.204950
13. R.B. Qiang, L.F. Hu, K.M. Hou, J.Q. Wang, and S.R. Yang, Water-Soluble Graphene Quantum Dots as High-Performance Water-Based Lubricant Additive for Steel/Steel Contact, *Tribol. Lett.*, 2019, **64**, p 67. https://doi.org/10.1007/s11249-019-1177-4
14. M.J. Fan, X. Du, L. Ma, P. Wen, S. Zhang, R. Dong, W.J. Sun, D.S. Yang, F. Zhou, and W.M. Liu, In Situ Preparation of Multifunctional Additives in Water, *Tribol. Int.*, 2019, **130**, p 317-323. https://doi.org/10.1016/j.triboint.2018.09.020
15. P. Wang, J. Qiu, P. Gao, R. Dong, Y. Han, and M. Fan, The Tribological Behaviors and Anti-corrosion Performances of 5-phenylte-trazole Ionic Liquid Additives for Water Lubricants, *Wear*, 2023, **516-517**, p 204621. https://doi.org/10.1016/j.wear.2023.204621
16. L.P. Xiong, Z.Y. He, S. Han, J. Tang, Y.L. Wu, and X.Q. Zeng, Tribological Properties Study of N-containing Heterocyclic Imidazoline Derivatives as Lubricant Additives in Water-Glycol, *Tribol. Int.*, 2016, **104**, p 98-108. https://doi.org/10.1016/j.triboint.2016.08.031
17. X.F. Wei, W. Li, X.Q. Fan, and M.H. Zhu, MoS_2-Functionalized Attapulgite Hybrid Toward High-Performance Thickener of Lubricating Grease, *Tribol. Int.*, 2023, **179**, p 108135. https://doi.org/10.1016/j.triboint.2022.108135
18. R.H. Xia, D. Lou, Y. Hammad, H. James, and H.H. Chen, Synergistic Effect of Hexagonal Boron Nitride and Carbon Nanofibers on Tribological Behavior of Nanolubricant, *Tribol. Int.*, 2023, **177**, p 107957. https://doi.org/10.1016/j.triboint.2022.107957

19. Y.X. Wang, Y.Y. Du, J.A. Deng, and Z.P. Wang, Friction Reduction of Water Based Lubricant with Highly Dispersed Functional MoS_2 Nanosheets, *Colloids Surf. A*, 2019, **562**, p 321-328. https://doi.org/10.1016/j.colsurfa.2018.11.047
20. J.M. Lineira del Rio, M.J.G. Guimarey, M.J.P. Comunas, E.R. Lopez, J.I. Prado, L. Lugo, and J. Fernandez, Tribological and Thermophysical Properties of Environmentally-Friendly Lubricants Based on Trimethylolpropane Trioleate with Hexagonal Boron Nitride Nanoparticles as an Additive, *Coatings*, 2019, **9**(8), p 509. https://doi.org/10.3390/coatings9080509
21. T.Q.P. Vuong, S. Liu, A. Van der Lee, R. Cusco, L. Artus, T. Michel, P. Valvin, J.H. Edgar, G. Cassabois, and B. Gil, Isotope Engineering of van der Waals Interactions in Hexagonal Boron Nitride, *Nat. Mater.*, 2018, **17**(2), p 152-158. https://doi.org/10.1038/NMAT5048
22. L. Reyes, A. Loganathan, B. Boesl, and A. Agarwal, Effect of 2D Boron Nitride Nanoplate Additive on Tribological Properties of Natural Oils, *Tribol. Lett.*, 2016, **64**, p 41. https://doi.org/10.1007/s11249-016-0778-4
23. Y.F. Bai, L.X. Wang, C.H. Ge, R. Liu, H.Y. Guan, and X.D. Zhang, Atomically Thin Hydroxylation Boron Nitride Nanosheets for Excellent Water-Based Lubricant Additives, *J. Am. Ceram. Soc.*, 2020, **103**(7), p 6951-6960. https://doi.org/10.1111/jace.17088
24. Z.S. Ma, H.L. Ding, Z. Liu, and Z.L. Cheng, Preparation and Tribological Properties of Hydrothermally Exfoliated Ultrathin Hexagonal Boron Nitride Nanosheets (BNNSs) in Mixed NaOH/KOH Solution, *J. Alloys Compd.*, 2019, **784**, p 807-815. https://doi.org/10.1016/j.jallcom.2019.01.108
25. F.S. Meng, Z. Li, H.H. Ding, J.S. Hu, W.J. Wang, J. Guo, and Q.Y. Liu, Study on the Preparation and Tribological Properties of BN@C-OA Nano-Additive Lubricants, *Wear*, 2021, **474-475**, p 203876. https://doi.org/10.1016/j.wear.2021.203876
26. M.K.A. Ali, X.J. Hou, L.Q. Mai, Q.P. Cai, R.F. Turkson, and B.C. Chen, Improving the Tribological Characteristics of Piston Ring Assembly in Automotive Engines Using Al_2O_3 and TiO_2 Nanomaterials as Nano-Lubricant Additives, *Tribol. Int.*, 2016, **103**, p 540-554. https://doi.org/10.1016/j.triboint.2016.08.011
27. Y.X. Cui, M. Ding, T.Y. Sui, W. Zheng, G.C. Qiao, S. Yan, and X.B. Liu, Role of Nanoparticle Materials as Water-Based Lubricant Additives for Ceramics, *Tribol. Int.*, 2020, **142**, p 105978. https://doi.org/10.1016/j.triboint.2019.105978
28. X.L. Wang and X.Y. Ye, Effect of Morphology on Tribological Properties of Fe_3O_4 as Lubricant Additive: Nanospheres, Nanowires and Nanosheets, *Tribol. Int.*, 2024, **191**, p 109201. https://doi.org/10.1016/j.triboint.2023.109201
29. J.H. Zhao, G.B. Yang, Y.J. Zhang, S.M. Zhang, C.L. Zhang, C.P. Gao, and P.Y. Zhang, Controllable Synthesis of Different Morphologies of CuO Nanostructures for Tribological Evaluation as Water-Based Lubricant Additives, *Friction*, 2021, **9**, p 963-977. https://doi.org/10.1007/s40544-020-0382-3
30. X. Zheng, Y. Xu, J. Geng, Y. Peng, D. Olson, and X. Hu, Tribological Behavior of Fe_3O_4/MoS_2 Nanocomposites Additives in Aqueous and Oil Phase Media, *Tribol. Int.*, 2016, **102**, p 79-87. https://doi.org/10.1016/j.triboint.2016.05.024
31. Y. Wang, Q.L. Wang, X.Q. Wei, Z.L. Song, Y. Lan, W.J. Luo, C.Q. Yin, Z.H. Yue, L. Zhou, and X.M. Li, A Novel Three-Dimensional Boehmite Nanowhiskers Network-Coated Polyethylene Separator for Lithium-Ion Batteries, *Ceram. Int.*, 2021, **47**(7), p 10153-10162. https://doi.org/10.1016/j.ceramint.2020.12.164
32. E.M. Ping, X.X. Chen, Y.S. Zhou, L.J. Zhang, L.Y. Kong, and N. Chen, H_2/D_2 Separation Using UTSA-16@CAU-10-H@γ-AlOOH Composites as the Stationary Phase in Gas Chromatography via the Additive Effects of Kinetic Sieving and Chemical Affinity Quantum Sieving, *Inorg. Chem.*, 2023, **62**(4), p 1591-1601. https://doi.org/10.1021/acs.inorgchem.2c03795
33. H.L. Zhang, P. Li, W.W. Cui, C. Liu, S.L. Wang, S.L. Zheng, and Y. Zhang, Synthesis of Nanostructured γ-AlOOH and Itsaccelerating Behavior on the Thermal Decomposition of AP, *RSC Adv.*, 2016, **6**, p 27235-27241. https://doi.org/10.1039/C5RA27838D
34. K. Saravanan, B. Shanthi, C. Ravichandran, B. Venkatachalapathy, K.I. Sathiyanarayanan, S. Rajendran, N.S. Karthikeyan, and R. Suresh, Transformation of Used Aluminium Foil Food Container into γ-AlOOH Nanoflakes with High Catalytic Activity in Anionic Azo Dye Reduction, *Environ. Res.*, 2023, **218**, p 114985. https://doi.org/10.1016/j.envres.2022.114985
35. W. Jang, S. Lee, N.R. Kim, H. Koo, J. Yu, and C.M. Yang, Eco-friendly and Scalable Strategy to Design Electrically Insulating Boron Nitride/Polymer Composites with High Through-Plane Thermal Conductivity, *Compos. B*, 2023, **248**, p 110355. https://doi.org/10.1016/j.compositesb.2022.110355
36. R. Zhang, L.C. Wang, J.Z. Ren, C.C. Hu, and B.L. Lv, Effect of Boron Nitride Overlayers on Co@BNNSs/BN-Catalyzed Aqueous Phase Selective Hydrogenation of Cinnamaldehyde, *J. Colloid Interface Sci.*, 2023, **630**, p 549-558. https://doi.org/10.1016/j.jcis.2022.10.117
37. T. Van Truong and D.-J. Kim, Synthesis of High Quality Boehmite and Gamma-Alumina for Phosphorus Removal From Water Works Sludge by Extraction and Hydrothermal Treatment, *Environ. Res.*, 2022, **212**, p 113448. https://doi.org/10.1016/j.envres.2022.113448
38. D. Yan, J. Li, M. Zahid, J.X. Li, and Y.Z. Zhu, Efficient Catalytic Selective Hydrogenation of Furfural to Furfuryl Alcohol Over Pt-supported on Surface Amino Functionalized Hexagonal BN Nanosheets, *Appl. Surf. Sci.*, 2023, **609**, p 155308. https://doi.org/10.1016/j.apsusc.2022.155308
39. Z. Salahuddin, S. Farrukh, R. Jan, A. Ayub, A. Hussain, M. Pontie, A. Ahmed, and M. Mubashir, Environmental Treatment and Remediation Using h-BN Based Smart and Hybrid Membrane, *Chemosphere*, 2022, **305**, p 135466. https://doi.org/10.1016/j.chemosphere.2022.135466
40. Y.Q. Bai, J. Zhang, Y.F. Wang, Z.Y. Cao, L.L. An, B. Zhang, Y.L. Yu, J.Y. Zhang, and C.M. Wang, Ball Milling of Hexagonal Boron Nitride Microflakes in Ammonia Fluoride Solution Gives Fluorinated Nanosheets that Serve as Effective Water-Dispersible Lubricant Additives, *ACS Appl. Nano Mater.*, 2019, **2**(5), p 3187-3195. https://doi.org/10.1021/acsanm.9b00502
41. H.J. Song, Z.Q. Wang, J. Yang, X.H. Jia, and Z.Z. Zhang, Facile Synthesis of Copper/Polydopamine Functionalized Graphene Oxide Nanocomposites with Enhanced Tribological Performance, *Chem. Eng. J.*, 2017, **324**, p 51-62. https://doi.org/10.1016/j.cej.2017.05.016
42. Q. Tian, X.H. Jia, Y.C. Zhang, Y.P. Zhang, J. Yang, S.Z. Wang, Y. Li, D. Shao, L. Feng, and H.J. Song, In-Situ Growth of Amorphous Carbon on Sucrose-Assisted Exfoliated Boron Nitride Nanosheets: Exceptional Water Dispersibility and Lubrication Performance, *Tribol. Int.*, 2022, **173**, p 107647. https://doi.org/10.1016/j.triboint.2022.107647
43. L. Zhang, Y. He, S.W. Feng, L. Zhang, L. Zhang, Z.L. Jiao, Y.Q. Zhan, and Y.J. Wang, Preparation and Tribological Properties of Novel Boehmite/Graphene Oxide Nano-Hybrid, *Ceram. Int.*, 2016, **42**(5), p 6178-6186. https://doi.org/10.1016/j.ceramint.2015.12.178
44. X.H. Jia, J. Huang, Y. Li, J. Yang, and H.J. Song, Monodisperse Cu Nanoparticles @ MoS_2 Nanosheets as a Lubricant Additive for Improved Tribological Properties, *Appl. Surf. Sci.*, 2019, **494**, p 430-439. https://doi.org/10.1016/j.apsusc.2019.07.194
45. U. Maurya and V. Vasu, Boehmite Nanoparticles for Potential Enhancement of Tribological Performance of Lubricants, *Wear*, 2022, **498-499**, p 204311. https://doi.org/10.1016/j.wear.2022.204311
46. L. Hao, W.D. Hao, P.P. Li, G.M. Liu, H.Y. Li, A. Aljabri, and Z.L. Xie, Friction and Wear Properties of a Nanoscale Ionic Liquid-like GO@SiO_2 Hybrid as a Water-Based Lubricant Additive, *Lubricants*, 2022, **10**(6), p 125. https://doi.org/10.3390/lubricants10060125